Zero-dimensional modelling of a producer gas-based reciprocating engine

G Sridhar*, **P J Paul,** and **H S Mukunda**
Combustion, Gasification, and Propulsion Laboratory, Department of Aerospace Engineering, Indian Institute of Science, Bangalore, India

Abstract: A zero-dimensional modelling study has been conducted using wrinkled flame theory for flame propagation to understand the in-cylinder pressure behaviour with time in a reciprocating internal combustion engine. These are compared with experiments conducted on the engine operated on biomass derived from producer gas and air mixture. The required inputs on the laminar burning velocity and turbulence parameters are obtained from separate studies. The data related to laminar burning velocity for producer gas and air mixture at thermodynamic conditions typical of unburned mixture in an engine cylinder were obtained from one-dimensional flame calculations. The turbulence parameters were obtained by conducting a three-dimensional computational fluid dynamics study on a bowl-in-piston geometry to simulate motored or non-firing conditions. The above mentioned data were used in the zero-dimensional model to make pressure–time (p–θ) computation over the complete engine cycle, for a range of test cases at varying compression ratio (CR) and ignition timing. The computational results matched reasonably well with experimental p–θ curves at advanced ignition timing at all CRs. The error in computed indicated power (IP) at advanced ignition setting ($18°$–$27°$ CA) is around 3–4 per cent for CR = 17.0 and 11.5, and between 6 and 9 per cent for CR = 13.5. However, at less advanced ignition setting, the error in computed IP is larger and this is attributed to enhanced fluid dynamic effect due to reverse squish effect. And, whenever major part of the combustion occurred during this period, the deviation in the computed result appeared to be larger. This model has also been used to predict output of a commercially available producer gas engine of 60 kW. The optimum ignition timing on this particular engine was experimentally found to be $22°$–$24°$ before top centre. The zero-dimensional model has been used in a predictive mode and results compared with brake power under wide throttle open condition.

Keywords: producer gas, zero-dimensional modelling, optimum ignition timing, compression ratio, derating

1 THE APPROACH

It is well recognized that the processes that govern the engine operation are extremely complex in nature. Although much is known about these processes, there is no adequate understanding from a fundamental point of view. Therefore, it is difficult to make predictions of engine operation based on governing equations alone. Empirical relations and *ad hoc* approximations are used to bridge this gap and these are argued as appropriate [1] till better understanding prevails over the underlying physics. An advantage of such empirical models is that they can be put to immediate use in areas of engine design and analysis. Therefore, thermodynamic or zero-dimensional model still continues to be popular among the engine designers [1, 2].

The work that is reported here is commensurate with the above thought process. This paper is a continuation of earlier work reported by the authors [3, 4]. In the current work, the zero-dimensional

**Corresponding author: Combustion, Gasification and Propulsion Laboratory, Department of Aerospace Engineering, Indian Institute of Science, Bangalore 560 012, India. email: gsridhar@cgpl.iisc.ernet.in*

JPE265 © IMechE 2006

Proc. IMechE Vol. 220 Part A: J. Power and Energy

model has been used in predictive mode and the output of a commercial gas engine predicted. The producer gas typically contains 18–20 per cent H_2, 18–20 per cent CO, 2–3 per cent CH_4, 12 per cent CO_2, 2.5 per cent H_2O, and N_2 as balance [5]. The lower calorific value of the gas is 5.2 ± 0.2 MJ/m^3, with a stoichiometry requirement of 1.2–1.4 kg of air for every kg of producer gas [5]. Stating the experimental work briefly, performance of spark ignited engines using producer gas derived from biomass has been studied. One set of experimental work was conducted on a multi-cylinder gas engine at varying compression ratio (CR) of 17, 14.5, 13.5, and 11.5 using producer gas fuel. The engine utilized for the study is a conversion of a production diesel engine, having the same cylinder and piston arrangement (bowl-in-piston) of the compression ignition engine. The relevant parameters such as the gas and air flowrates, gas composition, power delivered, and exhaust emissions were continuously monitored. The minimum advance for best torque (MBT) at CR of 17, 14.5, 13.5, and 11.5:1 has been identified as 6°, 10°, 14°, and 17° CA, respectively. Similarly, the in-cylinder p–θ data were obtained using a pre-calibrated (the calibration was conducted using rapid step functions of pressure generated by a pneumatic pressure pulse calibrator and readout on a oscilloscope) Piezo-based pressure transducer in steps of one crank angle (CA). The sensor is hermitically sealed (model no. HS 111A22) with a built-in charge amplifier, the other specifications being: resolution 0.69 kPa, rise time <1 μs, discharge time constant >500 s, and natural frequency of the crystal 550 kHz. The experimentally acquired p–θ curves were used for the validation of zero-dimensional computational results for a range of CRs and ignition timing. Further, the validated zero-dimensional model was used in predictive mode and the output of a commercial gas engine predicted. The engine data that were employed for zero-dimensional computation is a naturally aspirated (Cummins make, G743G model), natural gas engine (CR = 10), but operated on producer gas fuel. Performance evaluation showed that the 2.0 l engine developed a maximum brake output of 60 kW (Brake mean effective presure (BMEP) of 3.85 bar) at rated speed of 1500 r/min, corresponding to MBT timing of 22°–24° before top centre (BTC) [5].

2 THE ZERO-DIMENSIONAL MODEL

The model comprises of sub-models to simulate the four processes of reciprocating engine cycle, namely intake, compression, heat release followed by expansion and exhaust. The various sub-models used in the above simulation are (a) the filling and emptying technique for intake and exhaust processes, as outlined in Heywood [6], (b) Eddy entrainment and laminar burn-up (EELB) model for simulation of heat release, as derived by Keck [1], and (c) the heat loss due to convection based on Annand's convective heat transfer correlations, as discussed by Baruah [7]. The flame propagation (or heat release) is modelled as a two-zone model, where a thin wrinkled multi-connected laminar flame separates the burned and the unburned mixtures. The EELB model as formulated by Keck [1] is represented by two equations, namely

$$\frac{dm_b}{dt} = \rho_u A_f S_l + \frac{\mu}{\tau_b} \tag{1}$$

$$\frac{d\mu}{dt} = \rho_u A_f u_T - \frac{\mu}{\tau_b} \tag{2}$$

where $\mu = \rho_u \ell_T (A_\ell - A_f)$. Equation (1) represents the mass burn rate, whereas equation (2) represents the rate of change of mass of unburned mixture within the flame front. In these equations, there are two quantities, namely the characteristic speed (u_T) and length (ℓ_T), which could be related to the turbulence parameters, namely u' and I_I as identified in Heywood [6]. These turbulence parameters can either be determined using empirical correlations or from fundamental studies [6]. Keck [1] has provided empirical relationship for obtaining characteristic speed and length by coupling with few other variables related to engine geometry. Moreover, these correlations have been formulated for simpler geometries where turbulence is more dependent on the intake port design and less on the fluid–piston interaction inside the cylinder. Using the same correlation for complex geometries is not appropriate, since the flow is known to become substantially modified in the compression process. Therefore, a computational fluid dynamics (CFD) study was conducted on a cylinder–piston geometry (with bowl), simulating motoring condition for the complete engine cycle in one of the previous studies by the present authors [8]. Turbulence parameters, namely turbulence intensity and length scales, are extracted from the CFD results and used as a zero-dimensional model input. It was further assumed that during combustion, the unburned mixture undergoes isentropic compression sufficiently rapidly for the simple distortion process to occur as outlined in Heywood [6]. These are given as follows

$$u' = u'_0 \left(\frac{\rho_u}{\rho_0}\right)^{1/3}, \quad l'_I = l'_{I,0} \left(\frac{\rho_u}{\rho_0}\right)^{-1/3} \tag{3}$$

where ρ_u is the density of the unburned gas, ρ_0 the state at the start of combustion, u' and u'_0 the

turbulence intensity under reacting and non-reacting conditions, respectively, and I_l and I'_{l0} the integral length scale under reacting and non-reacting conditions, respectively.

Laminar burning velocity is another input parameter required for the heat release model. It was computed using an in-house code called 'FLAME CODE' [9] that uses a transient calculation procedure to compute one-dimensional laminar flame speed for a premixed flame. The code has been validated with experimental results [10, 11]. The fuel considered was of nominal composition with 20 per cent each of H_2 and CO, 2 per cent CH_4, 12 per cent CO_2, and N_2 as balance. Therefore, the theoretical burning velocity calculation has been done at varying equivalence ratio, initial temperature and pressure, and with varying amounts of external exhaust gas recycled (EGR) *ranging from 0 to 10 per cent*. The details of this part of the work are given in an earlier publications by the authors [12]. An expression for laminar flame speed derived from this analysis for fuel–air equivalence ratio between 0.9 and 1.3 is as given below

$$S_l(\text{cm/s}) = 94.35 \left(\frac{p}{p_0}\right)^{0.2744} [0.96 + 1.2(\Phi - 1)]$$
$$\times (1 - 2.4\psi) \qquad (4)$$

where p is the actual pressure during combustion in bar (abs), p_0 the reference pressure (1.0 bar), Ψ the external EGR fraction, and Φ the fuel–air equivalence ratio. The burning velocity dependence upon the initial temperature is built into the pressure term in equation (4). The burning velocity is about 30 per cent higher than that for the natural gas; it is also quite sensitive to the variations in H_2 and CO content that may occur naturally in the gasification process. A sensitivity analysis of variation in CO and H_2 content at an equivalence ratio (Φ) of about 0.9 revealed the burning velocity to reduce by about 7 per cent for reduction of every 1 per cent in H_2 or CO content.

3 DETAILS OF ZERO-DIMENSIONAL SIMULATION

The geometric details of the engines used for zero-dimensional simulation are given in Table 1. All the experimental measurements with respect to p–θ were conducted on engine E1 – a gas engine converted from the diesel engine at varying CR of 17, 13.5, and 11.5:1. Also, these results were utilized for initial validation of the zero-dimensional computational results. Therefore, in the initial part of the paper, the zero-dimensional computation results of engine E1 are presented. Later, the results of engine E2 at optimum ignition timing are presented. Prior to proceeding with the computation of firing p–θ curves, computations under motoring conditions were validated by comparing with the in-cylinder motoring curve recorded on the engine E1 [4]. The data used in zero-dimensional simulation are shown in Table 2. An important outcome of this motoring simulation was the estimation of charge trapped inside the cylinder at the closure of the intake valve. The motored pressure history was simulated using producer gas and air mixture and validated against the experimental p–θ curve in order to arrive at the realistic initial thermodynamic conditions. This validation procedure was followed at all CRs for engine E1. The possible error in pressure matching is well within 0.5 per cent for all the cases. The assumptions and features used in the zero-dimensional model are listed below

Table 1 Engine configuration details

Engine model	Diesel engine converted to gas engine (E1)	Cummins, G743G (E2)
Bore × stroke, mm	110 × 116	130 × 152
Number of cylinders	3	6
Compression ratio (CR)	17:1	10:1
Aspiration	Natural	Natural
Bumping clearance, mm	1.5	11
Combustion chamber	Flat cylinder head and cylindrical bowl-in piston	Flat cylinder head and shallow bowl-in piston
Squish area	70%	40%
Spark plug location	offset from centre of combustion chamber by 8 mm	Central
Valve lift, mm	11	10
Valve timing		
Inlet valve opening, BTC	26	10
Inlet valve closing, ATC	66	49
Exhaust valve opening, BBC	64	41
Exhaust valve closing, ATC	38	18

Table 2 Data for zero-dimensional simulation

| Wall temperature | 450 K |
| Simulation speed | 1500 r/min |

Annand coefficient for heat transfer [13] - $a =$

| | Compression and | |
Suction	expansion	Exhaust
0.2	0.8	0.4

Annand coefficient for heat transfer [13] - $b = 0.78$

| | Recycled gas mass fraction (%) with CR | | |
	Engine–E1		Engine–E2
17.0 CR	13.5 CR	11.5 CR	10.0 CR
6.5	7.5	8.5	8.5

Boundary condition	
Intake manifold	90 kPa and 300 K
Exit manifold	92 kPa and 300 K
Intake and exit valve [14]	$C_{d,}$ − 0.32 and 0.55

1. The gas exchange process was simulated by using filling and emptying technique. The values are given in Table 2.
2. All the four processes, namely gas exchange, compression, heat release, and expansion are simulated with heat loss, and mixture/product gas considered as perfect gas. The heat transfer coefficients used for different processes are listed in Table 2.
3. Subsequent to ignition occurring at a preset time, there is an apparent time delay in cylinder pressure rise due to combustion called the ignition delay. During the ignition delay period, the flame kernel is displaced from its point of formation.
4. The combustion during flame kernel formation is considered to occur under constant volume conditions, with products and mixture at different pressures.
5. With further movement of the flame, the heat release is simulated using EELB sub-model, wherein a spherical flame front (reaction zone) is assumed to propagate into the unburned mixture using a two zone model. Heat transfer is considered between individual zones and the combustion chamber walls.

The other assumptions on the heat release model are as discussed in Baruah [7]. The sub-models of the zero-dimensional model other than the heat release model are validated initially by comparing with the experimentally motoring p–θ curves. The primary information required to initiate the heat release effect is the ignition delay period that was estimated by superimposing the motoring curve over the experimental firing curve and taking the point of deviation ($\mathrm{d}p/\mathrm{d}\theta$ about 1.0 bar per unit crank angle) from the point of ignition as the delay period. The literature [6] indicates that during ignition delay period about

1 to 5 per cent of the initial mass is consumed, in this work about 1 per cent of the initial mass is assumed to have consumed, corresponding to a flame kernel of about 12 mm radius. The flame is assumed to move into the bowl during kernel formation; the dislodging of the flame from its point of ignition is well identified by Keck [1].

4 PROCEDURE FOR ZERO-DIMENSIONAL COMPUTATIONS

In these computations, appropriate fuel–air mixture recorded (the fuel gas is generated in a gas producer unit and supplied to the engine, the minor variation in the fuel gas composition and thereof the fuel-air mixture supplied to the engine is recorded) during experiments constitutes the input energy (IE). Dilution in terms of recycled gas fraction as depicted in Table 2 is considered at corresponding CRs. The recycled gas fraction in the total air and fuel mixture was calculated in the gas exchange process of the thermodynamic cycle simulating firing conditions. The necessary inputs for the heat release process are derived from separate computations as indicated earlier. Similarly, the equilibrium calculations for computing products and the adiabatic flame temperature are obtained using the SP-273 code of NASA [15]. The criterion for convergence is also highlighted, it is the stabilization of the peak cylinder pressure value, which needs to be within about 1.0 per cent in the successive cycles.

5 COMPUTATIONS OF P–Θ CURVE

The salient features of the 11 test cases for engine E1 (case 1 to 11) and one test case for engine E2 (case 12) are shown in Table 3, wherein the fuel gas

Table 3 Principal parameters of the test cases used in the zero-dimensional computations

| Case no. | CR | Composition (vol %) | | | Φ | I^a | Ign, °CA | Ign delay, °CA |
		H_2	CO	CH_4				
1	17.0	20.8	16.2	2.0	1.10	1.70	26	12
2	17.0	21.0	18.6	2.0	1.03	1.70	22	9
3	17.0	21.5	16	2.5	1.09	1.69	17	9
4	17.0	2.10	19.2	2.0	1.00	1.69	12	9
5	17.0	20.0	20.0	2.0	1.10	1.73	6	6
6	13.5	20.0	15.0	2.5	1.06	1.62	25	9
7	13.5	20.0	15.0	2.5	1.07	1.63	18	9
8	13.5	20.0	15.7	2.5	1.06	1.63	14	9
9	11.5	18.0	18.0	2.5	1.09	1.63	27	9
10	11.5	21.0	20.0	2.0	1.07	1.70	17	9
11	11.5	19.5	20.0	2.0	1.07	1.66	6	6
12	10.0	17.0	24.4	1.6	1.02	3.15	22	9

[a]I = Input energy/cycle, KJ.

Table 4 Principal results at more advanced ignition settings

		Experiment		Computation		
CR	Ign, ° CA	Peak Pr, bar	Occurrence, ° CA	Peak Pr., bar	Occurrence, ° CA	Duration, ° CA
17.0	26	60.9	366	60.8	365.8	43.4
17.0	22	64.4	366	63.0	366.4	39.6
13.5	25	46.3	368	44.8	367.2	60.0
13.5	18	36.9	372	36.8	371.0	56.0
11.5	27	38.0	368	35.2	367.6	68.0

composition, fuel–air equivalence ratio without recycled gas (EGR), input energy per cycle, set ignition timing, ignition delay are highlighted. In Table 3, case 1 (in italics) corresponding to an ignition advance of 26° CA at CR = 17.0 was used as a trial case for choosing the coefficients for the heat loss equation. The coefficients chosen for the four processes of the engine cycle are given in Table 2. The computed p–θ curve and the integrated value of pressure–volume curves are discussed subsequently.

6 RESULTS

6.1 Computations with advanced ignition setting

The results of five test cases (cases 1, 2, 6, 7, and 9) belonging to three CRs of engine E1 are shown in Table 4. The ignition settings of these cases are between 18 and 27° CA. The case 1 represented in italics is essentially used as a trial case for choosing the coefficients for the heat loss equation. All the four cases are computed with the well-observed phenomenon of a spherical flame propagating into the unburned mixture. With the ignition occurring at the pre-set time, a flame kernel forms at the ignition site. During the ignition delay period, the flame kernel is assumed to move vertically downward due to the surrounding turbulent fluid flow. Subsequent to the ignition delay period, the EELB model of flame propagation is invoked, wherein a spherical flame is assumed to propagate into the unburned mixture, with continued movement of the flame due to local fluid velocities. This spherical flame propagation continues till the flame encounters a wall, further the entrained unburned mixture is assumed to burn exponentially [1]. During the quasi-steady flame propagation, typical turbulent burning velocities are of the order of 7–9 m/s (at CR = 17.0) and time scale of the order of 0.5–0.6 ms during the initial stages of flame propagation, and once the flame reaches the wall, time scale for exponential burning is of the order of 0.8 to 1.0 ms and somewhat similar to the value (0.6 to 1.0 ms) reported by Keck [1]. Using this theory, computations for four test cases have been attempted. The

simulation scheme is organized to calculate the complete engine cycle, till successive cycles converge. The first cycle simulation is done by assuming a recycled gas of 12 per cent H_2O, 14 per cent CO_2, and N_2 as balance. Two more cycles are subsequently attempted using the product gases obtained from the equilibrium calculations as the recycled gas. These computations are attempted with a time step of 0.2° CA (0.022 ms) and confirmed to be time step independent. The computations for two of the four test cases are shown in Figs 1 and 2. The principal results are given in Table 4. The computed results at CR = 17.0 corresponding to an ignition advance of 22° CA match excellently with the experimental data, with marginal variation in the peak pressure and its point of occurrence. In the computations at CR = 13.5 at an ignition advance of 25° CA, the pressures are marginally higher at the commencement of heat release, with peak pressure falling short of the experimental value by about 1.5 bar and as a consequence the expansion pressures are lower. However, computation at 18° CA ignition advance matched reasonably well with the experimental data even though the computed pressure deviates after about 356° CA. The predicted duration of combustion is shorter at retarded ignition setting implying faster burn rate. Similar is the case with computations at CR = 11.5 at an ignition advance of 27° CA.
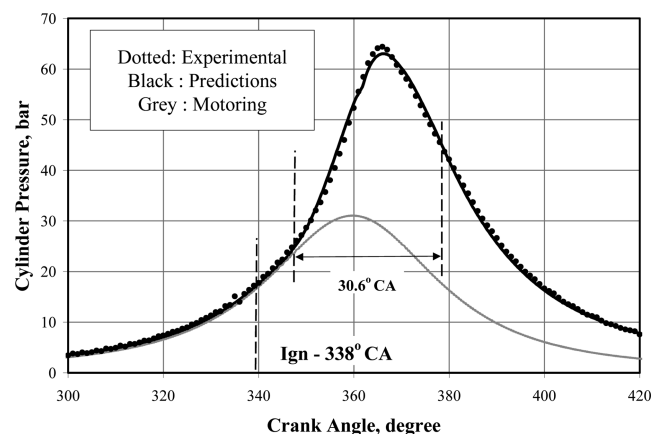

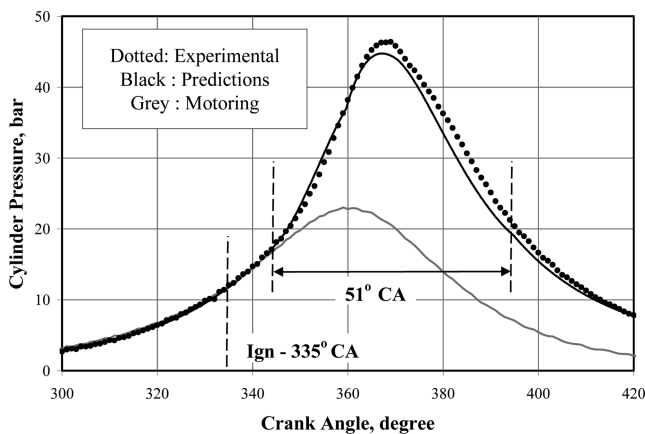**Fig. 1** p–θ computation at 22° CA ignition advance at CR = 17.0

Fig. 2 p–θ computation at 25° CA ignition advance at CR = 13.5

6.2 Computations with less advanced ignition setting

The results of six test cases corresponding to less advanced ignition setting are shown in Table 5. Computations using spherical flame assumption were made for all the six test cases, one test result corresponding to CR = 17 at 12° CA ignition advance is shown in Fig. 3. The principal results are given in Table 5. From Fig. 3, it is evident that there is deviation in the computed pressures beyond a CA. At careful look at the experimental curve shows that there is a steep rise in the cylinder pressure, giving an impression of auto-ignition. However, this is not true because if auto ignition were to occur then it should have occurred even at advanced ignition timing, wherein the thermodynamic condition is of the same severity. In fact, the engine has been tested between ignition timing of 33 and 6 BTC and no knock (either from the pressure data or from noise) has been observed. The pressure rise between ignition advance of 33 and 17 CA has been found to be gradual and matched well with the computational results. Similarly, HCCI could be ruled out because as a part of measurement a 'grab' motoring test was conducted on the instrumented cylinder (with piezo sensor) under wide-open throttle condition by rapidly switching from firing to motored condition (the ignition to the cylinder fitted with the pressure sensor was cut-off and pressure data acquired). The maximum cylinder pressure was identical to the motoring pressure at wide-open throttle condition. Had there been HCCI, then the pressure should have been higher, which has not been the case so. The possible cause for the discrepancy between the experimental and computation results at less advanced or retarded ignition timing is brought out in the following paragraphs.

Coming back to the computation results, it is not immediately obvious as to why there is a deviation beyond a certain point. The deviation in pressure might be occurring as a result of increased burn rate either due to enhanced surface burning area or the enhanced entrainment. Higher surface area for burning is possible provided the flame does not quench at the surrounding walls and the flame remains floating. This calls for the displacement of the spherical flame in a more complex manner than what has been accounted in this analysis. However, considering, this effect had marginal effect on the maximum pressure rise. This behaviour was found to be similar with all the six test cases. Therefore, at less advanced ignition setting, the enhanced fluid dynamics due to reverse squish flow could be modifying the burn rate to such an extent that there is a steep rise in cylinder pressure. The cold flow CFD studies [8] clearly indicate high velocity jets coming out of the bowl and reentering the cylinder during reverse squish period. And, whenever major part of the combustion occurred during this time, there appears to be abrupt increase in the burn rate leading to steep pressure rise. This effect appears to be more severe in for higher CR of 17 and 13.5 when compared with CR = 11.5. This could be true because the peak reverse squish velocities with CR = 17 is of the order of 31 m/s as against 6 m/s for CR = 11.5 [8]. Therefore, the deviations in the computed results at CR = 11.5 is lower when compared with CR = 17 and 13.5. The integrated values of pressure–volume data over a complete cycle resulting in indicated power (IP) are presented in Table 6. At advanced ignition timing,

Table 5 Principal results of at less advanced ignition setting

CR	Ign, ° CA	Experiment			Computation		
		Peak Pr, bar	Occurrence, ° CA		Peak Pr., bar	Occurrence, ° CA	Duration, ° CA
17.0	17	67.4	369		52.0	370.8	37.2
17.0	12	75.6	369		47.1	372.4	37.4
17.0	06	54.5	379		39.2	375.0	35.4
13.5	14	45.0	376		33.2	373.2	52.6
11.5	17	37.5	372		30.5	373.0	48.4
11.5	06	25.0	383		24.0	377.6	52.0

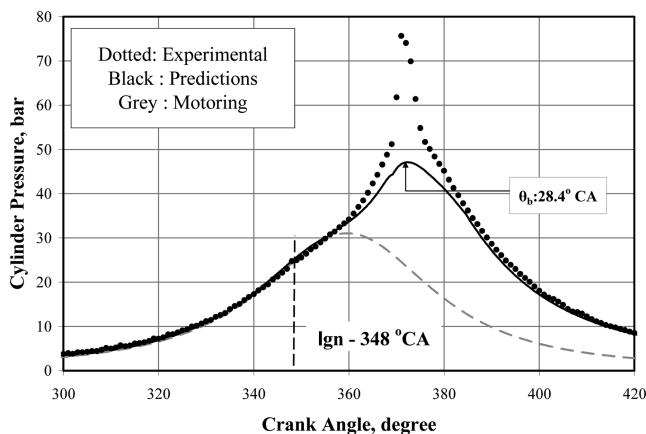**Fig. 3** p–θ prediction at $12°$ CA ignition advance at CR = 17.0

the zero-dimensional model is able to make reasonably good predictions by assuming the conventional spherical flame propagation model. The accuracy in IP prediction is around 3 per cent for CR = 17.0 and 11.5, and between 5 and 8 per cent for the other two cases at CR = 13.5. In all the 11 test cases that were discussed, for higher CR of 17 and 13.5, the error in the zero-dimensional prediction is large in around ignition advance of 6 and $12°$ CA, respectively. Whereas, for lower CR = 11.5, the error in zero-dimensional prediction is of the order of 5–6 per cent. Sensitivity analysis was conducted for test case corresponding to CR = 17 at an ignition setting of $22°$ CA. 10 per cent variation in laminar burning velocity and turbulence intensity has very little influence on the IP. The zero-dimensional model has the drawback that it cannot take into the fluid flow; therefore, a detailed three-dimensional CFD modelling would be essential to understand the phenomenon.

Table 6 Summary of zero-dimensional computations for different test cases

Case no.	CR	Ign, CA	IP[a] – Exp, kW	IP[a] – 0-D, kW	% error
1	17.0	26	19.5	19.1	2.0
2	17.0	22	21.3	20.6	3.2
3	17.0	17	22.3	20.4	8.5
4	17.0	12	24.1	20.7	14.0
5	17.0	6	24.2	19.8	18.0
6	13.5	25	19.6	18.4	6.0
7	13.5	18	19.9	18.1	9.0
8	13.5	14	21.4	18.2	15.0
9	11.5	27	18.2	17.4	4.3
10	11.5	17	19.9	18.6	6.5
11	11.5	6	19.3	17.6	9.0

[a]Net indicated power.

7 ZERO-DIMENSIONAL COMPUTATIONS FOR ENGINE E2

Considering the success of zero-dimensional prediction at lower CR, the zero-dimensional model has been extended to engine E2 of CR = 10. The combustion chamber of engine E2 is also of bowl-in piston configuration, but is shallower compared to engine E1. The squish ratio of about 40 per cent compared to 70 per cent is the earlier case. Similarly, the engine is provided with two intake and two exhaust valves instead of one each in the earlier case. The zero-dimensional model has been applied on the above geometry with the following additional assumptions: (a) the values of turbulence parameters was considered to be same as that of engine E1 corresponding to CR = 11.5, (b) since the valve lift profile (but the valve lift of the engine is known and is 10 mm) for engine E2 was not available, the valve lift profile of engine E1 was considered, and (c) an ignition delay of $9°$ CA was considered based on studies on engine E1. The fuel–air mixture composition considered for computation is shown in Table 3. These values were recorded during the long duration trials on the engine. The engine had developed a maximum brake output of 60 kW at an optimum ignition setting of $22°$–$24°$ BTC. Therefore, computation has been attempted corresponding to optimum ignition setting of $22°$ and $24°$ BTC. For the first cycle calculation, only fuel–air mixture (without recycled gas) was considered. In the subsequent cycles, the recycled gas fraction in the total air and fuel mixture was calculated in the gas exchange process, the amount of recycled gas was computed to be around 8.5 per cent. Here, it is important to note that the recycled gas fraction is comparable with engine E1 at CR = 11.5, even though the CR of engine E2 is lower. This higher scavenging efficiency appears to be due to two intake and exit valves and has been captured by the gas exchange sub-model. The computed p–θ for two ignition settings is shown in Fig. 4. There is marginal variation in the IP between $22°$ and $24°$ CA ignition timing. The computed IP_{Gross} was 76 kW and 76.5 kW at $24°$ and $22°$ CA ignition timing, respectively. The peak pressure was computed to occur at $373.4°$ and $377.6°$ CA for ignition setting of $24°$ and $22°$ CA, respectively. It is well identified in the literature [6] that MBT corresponds to a value wherein the peak cylinder pressure should occur at $376°$–$377°$ CA. Therefore, $22°$ CA could be considered as the MBT for E2 based on computation. There are few uncertainties involved with respect to these computations and they are: (a) turbulence parameters could be different considering the variation of the bowl geometry, (b) under-estimation of the
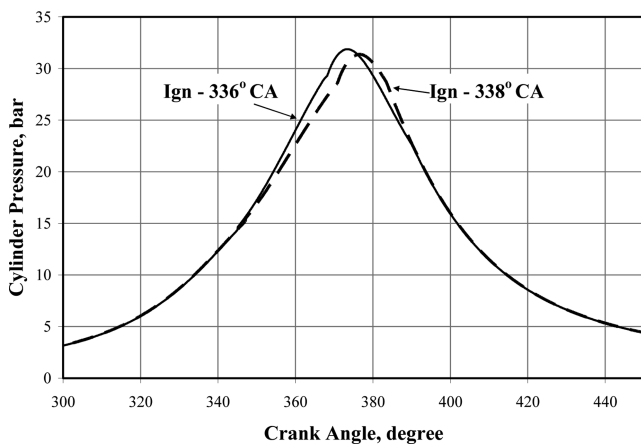
Fig. 4 $p-\theta$ prediction at two ignition timings for E2

input energy to the engine – variation in gas calorific value to an extent of 5 per cent, (c) incorrect valve lift profile chosen resulting in computed pumping loss to be higher, and (d) uncertainty in the power consumed by accessories. In the results presented in Table 7, the net brake power (BP) has been computed after deducting the pumping loss, frictional loss – rubbing and power consumed by accessories (fan). The frictional power (FP) – rubbing, has been estimated from Willans line. The power consumed by the accessories (fan) is based on data from Cummins [**16**].

Computational results are shown in Table 7 with and without some of these uncertainties as cases I and II, respectively. The results with some of the above uncertainties are shown as case I in Table 7. The uncertainties considered are with respect to energy input and pumping loss. A higher input energy of 5 per cent resulted in an IP of 78.2 kW. Similarly, if one extends the pumping loss results of engine E1, wherein the pumping loss is about 0.27 kW per unit swept volume of the cylinder, the pumping loss for engine E2 works to about 4.5 kW as against 6.5 kW computed originally. Results without the above mentioned uncertainties are shown in the case II of Table 7, wherein the difference is about 5–6 per cent.

8 CONCLUSIONS

Summarizing the zero-dimensional computation qualitatively, in the limited number of test cases

Table 7 Results for engine E2 at 22° CA

Case	IP$^a_{Gross}$ (kW)	Pumping^a loss (kW)	FP^b (kW)	Fan^c (kW)	BP (kW)	Difference ± %
I	78.2	4.5	4.0	9.2	60.5	+1.0
II	76.5	6.5	4.0	9.2	56.8	−5.5

^{a}0-D model.
^{b}Willans line.
^{c}Cummins data.

that were attempted, the zero-dimensional model is able to make reasonably accurate predictions at advanced ignition settings (above 17° BTC) using classical EELB heat release sub-model. However, at less ignition setting (<17° BTC), the enhanced fluid dynamics due to reverse squish flow modifies the burn rate to such an extent that there is a steep rise in cylinder pressure. By making use of the insight obtained from the cold flow CFD studies, it appears that the flame shape is modified during the reverse squish period. Therefore, fluid–flame interaction is sufficiently complex and predictions with simpler techniques like zero-dimensional model are not possible. This calls for a full-fledged three-dimensional modelling with combustion for further understanding. However, with zero-dimensional model providing reasonably accurate predictions, the model needs to be further validated for various engine geometries.

APPENDIX

Notation

A_f, A_l	spherical flame and laminar burning area (m^2)
I_I, I'_{I0}	integral length under reacting and non-reacting condition (m)
ℓ_T	characteristic length (m)
m_b	mass of mixture burned (kg)
p, p_0	actual cylinder pressure and reference pressure (bar)
S_l	laminar burning velocity (m/s)
u', u'_0	turbulence intensity under reacting and non-reacting condition (m/s)
u_T	characteristic speed (m/s)
μ	parametric mass (kg)
ρ_u	unburned gas density (kg/m^3)
ρ_0	unburned gas density at the start of combustion (kg/m^3)
τ_b	characteristic time (s)
Φ	fuel-air equivalence ratio
Ψ	recycled gas fraction

REFERENCES

1 **Keck, C. J.** Turbulent flame structure and speed in SI engines. Proceedings of 19th international Symposium on Combustion, 1982, pp. 1451–1466 (Combustion Institute, USA).

2 **Maly, R. R.** State of the art and future needs in SI engine combustion, Proceedings of 25th International Symposium on Combustion, 1994, pp. 111–124 (Combustion Institute, USA).

3 **Sridhar, G., Paul, P. J.,** and **Mukunda, H. S.** Experiments and modeling of producer gas based

reciprocating engines. In Proceedings of 2002 Fall Technical Conference of The ASME IC Engines Division, New Orleans, USA, 2002, ICE-vol. 39, pp. 377–388, No. ICEF2002-520.

4 **Sridhar, G.** *Experimental and Modelling studies of producer gas based spark-ignited reciprocating engines.* PhD Thesis, Indian Institute of Science, 2003.

5 **Sridhar, G., Sridhar, H. V., Dasappa, S., Paul, P. J., Rajan, N. K. S.,** and **Mukunda, H. S.** Development of producer gas engines. *Proc. IMechE, Part D: J. Automobile Engineering*, 2005, **219**, 423–438.

6 **Heywood, J. B.** *Internal combustion engine fundamentals*, International edition, 1988 (McGraw-Hill, Singapore).

7 **Baruah, P. C.** Combustion and cycle calculations in SI engines. The *thermodynamics and gas dynamics of IC engines*, vol. 2, 1986, pp. 823–865.

8 **Sridhar, G., Paul, P. J.,** and **Mukunda, H. S.** Simulation of fluid flow in high compression ratio reciprocating IC engine. *Proc. Instn Mech. Engrs, Part A: J. Power and Energy*, 2004, **218**, 403–416.

9 **Lakshmisha, K. N.** *Computational studies on the flammability limits of premixed gases.* PhD Thesis, IISc, 1991.

10 **Kanitkar. S., Chakravarty, P., Paul, P. J.,** and **Mukunda, H. S.** The flame speeds, temperature and limits of flame propagation for producer gas–air mixtures. In Proceedings of 4th National Meet on *Biomass gasification and combustion*, Mysore, India, 1993, vol. 4, pp. 50–62.

11 **Chakravarthy, P., Mishra, D. P., Paul, P. J.,** and **Mukunda, H. S.** The theoretical calculations of the limits of flame propagation for producer gas mixture. In Proceedings of 4th National Meet on *Biomass gasification and combustion*, Mysore, India, 1993, vol. 4, pp. 28–37.

12 **Sridhar, G., Paul, P. J.,** and **Mukunda, H. S.** Computational studies of laminar burning velocity of a producer gas and air mixture at typical engine conditions. *Proc. IMechE, Part A: J. Power and Energy*, 2005, **219**(A3), 195– 202.

13 **Annand, W. J. D.** Heat transfer in the cylinders of R/c IC engines. *Proc. Instn Mech. Engrs*, 1963, **177**, 973–990.

14 **Bicen, A. F., Vafidis, C.,** and **Whitelaw, J. H.** Steady and unsteady air flow through the intake valve of R/c engine. *J. Fluid Eng., ASME*, 1985, **107**, 413–426.

15 **Gordon** and **McBride.** *Method of calculating equilibrium composition, adiabatic flame temperature, rocket performance and detonation.* NASA SP 273, 1975.

16 *Gas engine manual.* Bulletin no. 3243676–04, April 2003 (Cummins India Ltd., Pune, India).